UC Berkeley

UC Berkeley Previously Published Works

Title

Forecasting groundwater levels using machine learning methods: The case of California's Central Valley

Permalink

https://escholarship.org/uc/item/34f8s9bt

Authors

May-Lagunes, Gabriela

Chau, Valerie

Ellestad, Eric

et al.

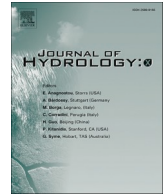## Publication Date

2023-12-01

DOI

10.1016/j.hydroa.2023.100161

Copyright Information

This work is made available under the terms of a Creative Commons Attribution License, available at https://creativecommons.org/licenses/by/4.0/

Peer reviewed

Research papers

Forecasting groundwater levels using machine learning methods: The case of California's Central Valley

Gabriela May-Lagunes [a,b,*], Valerie Chau [a], Eric Ellestad [a], Leyla Greengard [a,*], Paolo D'Odorico [b], Puya Vahabi [a], Alberto Todeschini [a], Manuela Girotto [b]

[a] *University of California, School of Information, Berkeley, CA 94720, USA*
[b] *University of California, Department of Environmental Science, Policy and Management, Berkeley, CA 94720, USA*

ABSTRACT

Groundwater, the second largest stock of freshwater on the planet, is an important water source used for municipal water supply, irrigation, or industrial needs. For instance, California's arid Central Valley relies on groundwater resources to produce a quarter of the United States' food demand as farmers rely on this precious resource when surface water is scarce. Despite its importance, the nexus between groundwater dynamics and climate drivers remains difficult to quantify, model, and predict because of the lack of a comprehensive observation network. In this study, machine learning techniques were used to predict groundwater levels with a 3-month forecasting horizon for the Sacramento River Basin. For this, publicly available meteorological and hydrological datasets and in-situ well-level measurements were used. Time series, ensemble-based, and deep-learning models including transformers were all tested, with an ensemble-based, XGBoost model, producing the best mean standard deviation percent error (MSPE) of 32.23% and a root mean squared error (RMSE) of 1.05 m (m) when using a 3- month forecasting horizon and when tested using a monthly rolling window over the years 2017–2020. The model proved to be better at predicting into wet months than the dry summer months and was found to be better at extracting seasonality than explaining well-level residuals, with well-specific features, as opposed to exogenous meteorological features specific to the hydrological unit of the well, ranking as the most important features to the model. Though other forecasting horizons were tested, a 3-month look-ahead window resulted in the best balance of precision and accuracy, where smaller forecasting horizons resulted in smaller RMSE but larger MSPE scores and vice-versa for larger forecasting horizons.

1. Introduction

Aquifers account for a major freshwater stock on Earth and provide a natural reservoir to modulate the effect of seasonal and interannual fluctuations of precipitation on water re- source availability. Groundwater is used by human societies for a variety of needs, including municipal water supply, irrigation, and industrial operations. In many regions of the world irrigation strongly relies on groundwater, often leading to unsustainable water withdrawals (or'overpumping') and groundwater depletion (Wada et al., 2016; Taylor et al., 2016; Rosa et al., 2018). Thus, the management of groundwater resources is of great strategic, economic, and environmental importance. Improved groundwater management hinges, among other factors, on adequate

observation, understanding, and prediction of groundwater dynamics, which often remain difficult tasks because of the dearth ofmeasurements and the lack of knowledge of the geological properties of aquifers. Therefore, there is often a very limited ability to develop process-based hydrological models of groundwater recharge and water table dynamics. This study utilizes machine learning techniques to create a model that can predict groundwater levels three months in advance to aid in water management.

Previous successful attempts to develop machine learning models of groundwater levels in different target regions haveused time series, ensemble, and deep learning models (Tao et al., 2022). The majority of the input parameters in these models are based on the history of the groundwater levels. In other words, previous models mostly used auto-
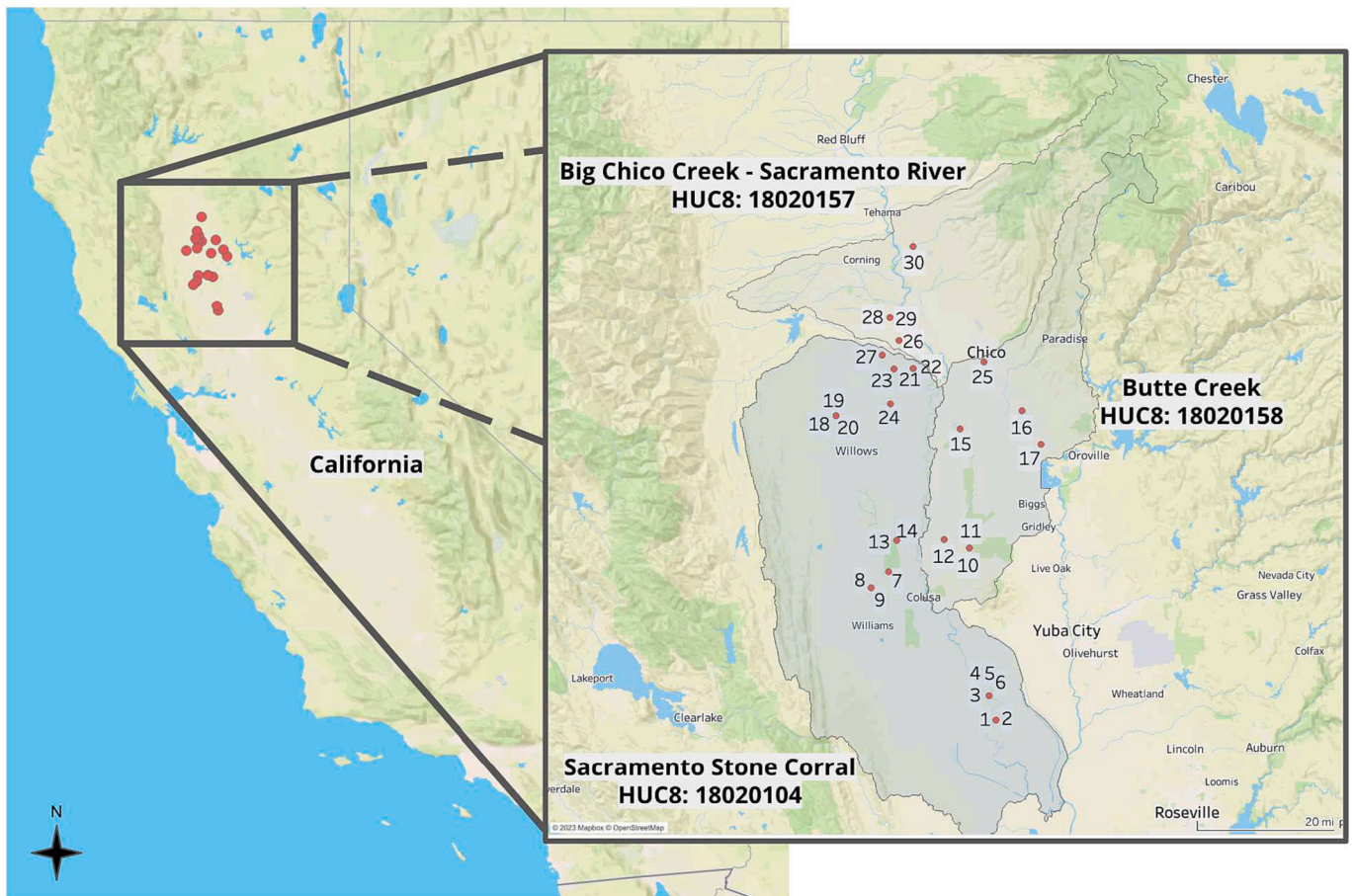
Fig. 1. Sample of wells used in this study and their hydrological region codes (HUC8 (USGC, 2023). Each well is marked with a unique identification (id) number that was arbitrarily assigned for this work. Table A2 (see Appendix) lists the California Natural Resource Agency's unique station code of each well id. Wells are seen in clusters due to nested structure of most wells.

correlated inputvariables (Tao et al., 2022) with only a few (or none) exogenous meteorological and hydrological training data (or 'features') (Barzegar et al., 2017). Nevertheless, there have also been some well-performing models (Tao et al., 2022; Barzegar et al., 2017) that use input variables such as temperature, surface runoff, evaporation, precipitation, surface water level and pumping rates (Tao et al., 2022; Barzegar et al., 2017).

Here a readily-applicable groundwater model was developed open-source data to predict groundwater levels in the Central Valley's Sacramento River watershed. This study limited to the Sacramento River basin due to the lack of data from other basins in the Central Valley. The Sacramento basin region is an ideal case study as it accounts for one-third of the Central Valley, which is a major food-producing region that is prone to droughts. Here in-situ measurements of well water levels in this region were modeled and predicted. To that end, different machine learning algorithms were used and classified into three different categories: time series models, ensemble-based models, and deep learning models. There was improvement upon previous studies by using a larger range of meteorological and hydrological variables (or 'features') that are known to affect groundwater levels, including snow water equivalent (SWE) (Li and Rodell, 2021) and evapotranspiration (ET) (Condon et al., 2020). The full list of the final features can be seen in appendix A.1.

Even though different machine learning algorithms were evaluated, all experiments in this work followed the same principal assumptions. First, it was assumed that the introduction of SWE as an input variable would increase the learning and forecasting capability of the models, thus allowing them to perform better than previous models where this

feature was not introduced. This was assumed because of the effect of SWE within the water cycle. Second, it was assumed that evapotranspiration would be a good proxy for agricultural activity such as irrigation. Third, the effects of other human activities on groundwater levels in the wells were assumed to be sufficiently small to allow for a good forecasting capability using only meteorological features.

Prior to this work, other studies have modeled and forecasted groundwater levels in different regions of the world, using a wide variety of machine learning algorithms (Tao et al., 2022). In this project advances research in this field by making three major methodological changes. First, the input variables here used were chosen to try to model the hydrologic response as closely as possible. Previous methodologies have focused their efforts in modeling the groundwater level evolution based on historical groundwater levels and their autocorrelation. In other words, they focused on univariate time series analyses (Goodarzi, 2020; de Moraes Takafuji et al., 2019). Other works have used exogenous input variables (i.e., other hydroclimatic variables different from groundwater levels), but they limited their input variables to precipitation, temperature, humidity, and evapotranspiration, which do not provide a complete representation of the water balance (Ebrahimi et al., 2022; Zhang et al., 2023). This study uses a more complete set of input variables that play an important role in groundwater dynamics in this region, including snow water equivalent (SWE). For a complete list of variables used see A1.

It is hypothesized that models such as tree-based algorithms and neural networks will be able to learn from the complex between groundwater levels and these hydrological variables, allowing the model to learn the underlying patterns and improve its forecasting capabilities.
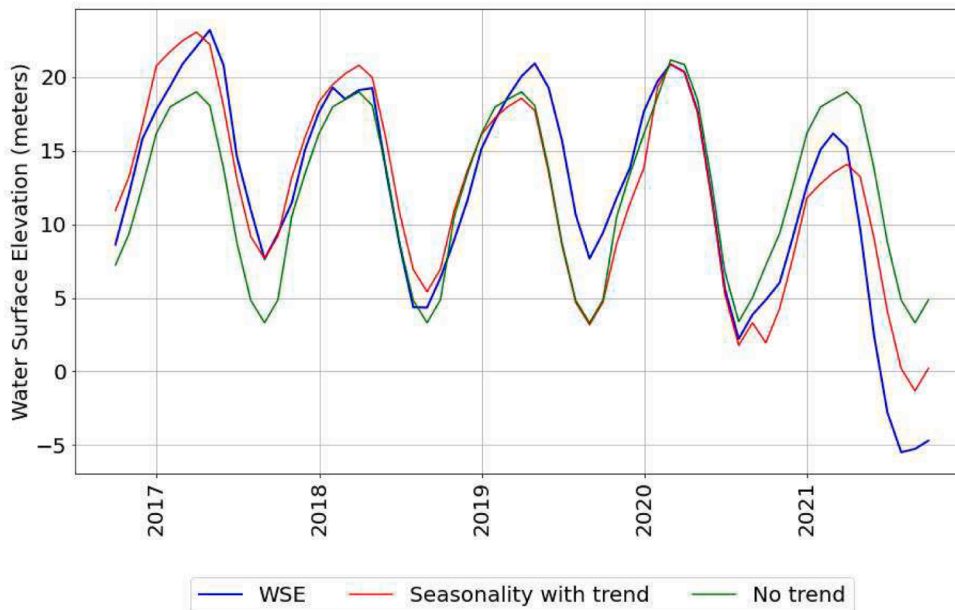
(a) Well 28
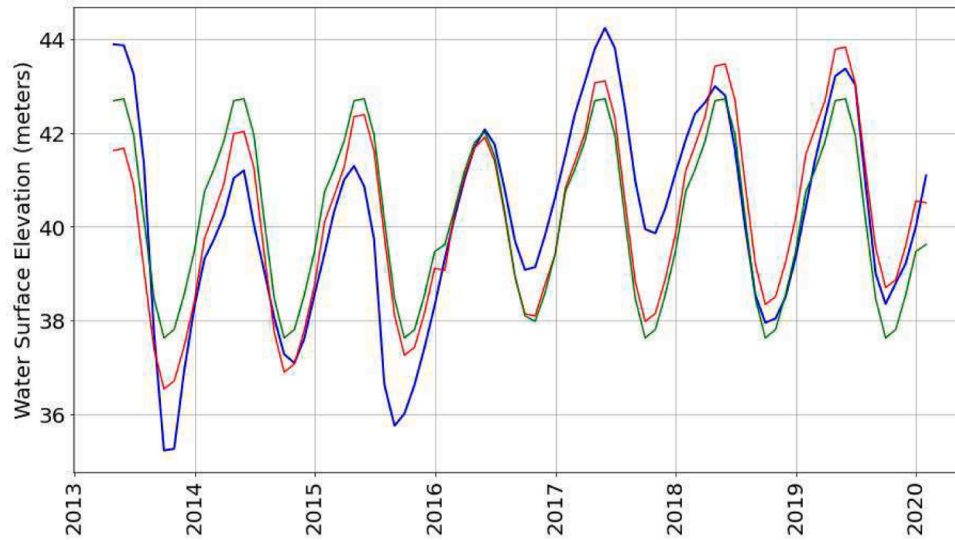
(b) Well 19

Fig. 2. Examples Water Surface Elevation (or water table height, WSE) time series for a) Well id: 28, b) Well id: 19.

It was assumed that the fluctuation of the groundwater levels observed in the wells was a combination of seasonal variability and sporadic events that meteorological data cannot fully explain, likely due to human intervention. To address this point, the seasonality residuals were extracted and used as explained later. Finally, the proposed methodology has the capability of being transferred to any region of interest in the world thanks to the exclusive use of input variables from open-access and global datasets, as explained in the experimental set up section.

2. Materials and methods

2.1. Study region

This study concentrates on groundwater resources in California's Central Valley. In this region, the rate of groundwater depletion has been accelerating since 2003 (Liu et al., 2022) due to climate change and an increasing demand for irrigation. In fact, higher temperatures enhance evapotranspiration crop water needs, preventing adequate groundwater recharge. California's Central Valley is of particular interest as it produces 25 % of the USA's food supply, with an annual value of ≈ 17 billion (Faunt et al., 2009, 1766). The Central Valley uses both surface water and groundwater for farming, though multiyear droughts have exacerbated the strain on limited groundwater resources. Roughly 75 % of the irrigated land in California and 17 % of the US's irrigated land is in the Central Valley; approximately 20 % of the US's groundwater demand is supplied from pumping Central Valley aquifers (Faunt et al., 2009). This makes the Central Valley's aquifer system the second most-pumped in the USA. As such, California's Central Valley has become reliant on groundwater resources, requiring unsustainable
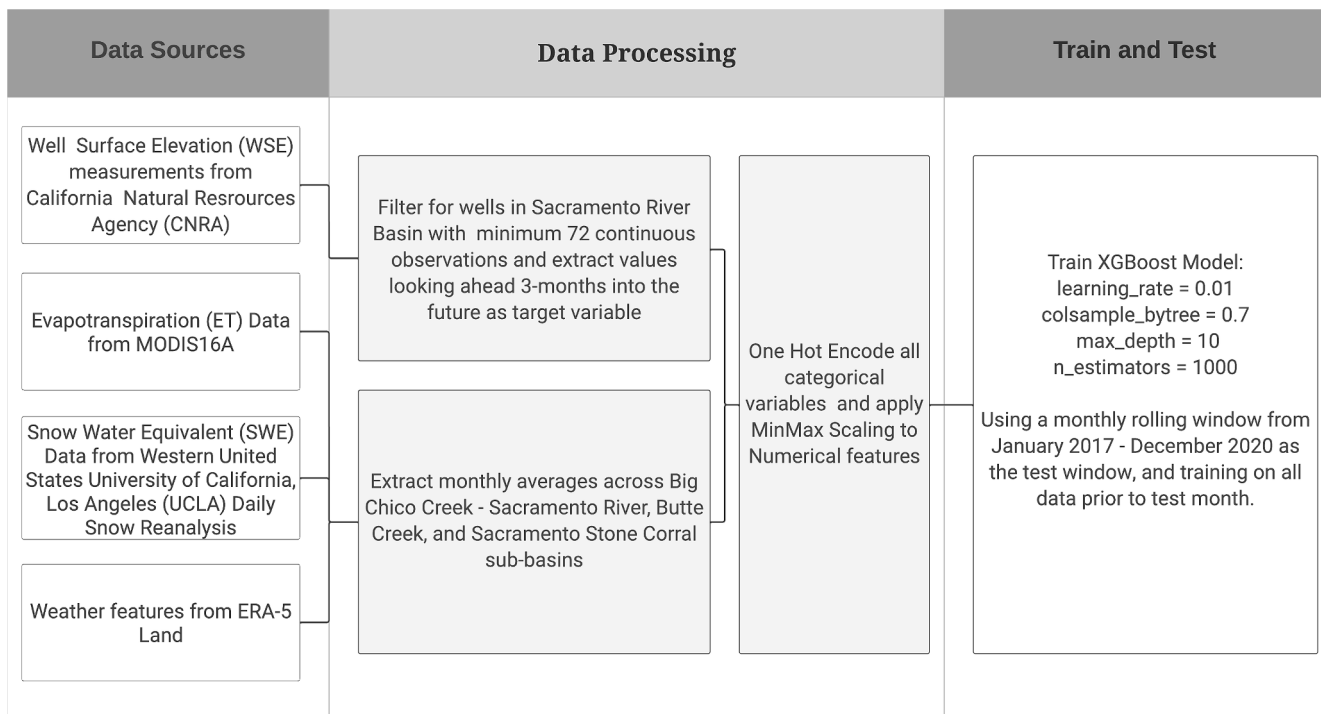
Fig. 3. Flowchart showing data sources for features and target variables and data processing applied. Further information on feature definition and feature engineering can be found in section 2.3.6 and in Appendix 1–3. N.B. One-hot encoding and MinMax scaling are standard data pre-processing practices. More information about these can be found in the references (Hancock, 2020). Note that the model predicts values 3-months into the future, so the month of the test period (January 2017) is predicting Well Surface Elevation (WSE) values for April 2017. The datasets used as input are open source and can be found here: WSE (California Natural Resources Agency, CNRA) (CNRA, 2023), ET (MODIS16A) (Running et al., 2022), SWE(UCLA Daily Snow Reanalysis) (Fang et al., 2022), weather features(ERA-5 Land) (Store).
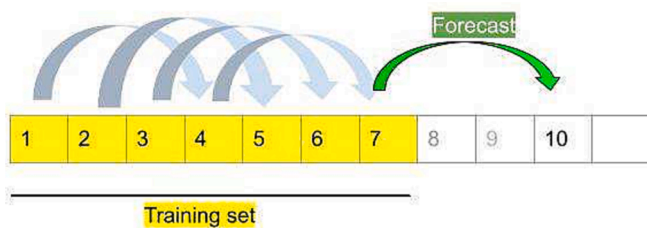

Fig. 4. The training set connects each observation with the water surface elevation (WSE) three months ahead. For example, to predict month 8, WSE observations from months 1 to 4 are used for training, while month 5 is the test set. Similarly, to predict month 9, observations from months 1 to 5 are the training set, and observation 6 is the test set. For month 10, observations from months 1 to 6 are the training set, and observation 7 is the test set (green arrow). The error is the average of the WSE prediction errors for months 8, 9, and 10. During training, geographical and meteorological data for each month are matched with the WSE value three observations later (grey arrows). (For interpretation of the references to colour in this figure legend, the reader is referred to the web version of this article.)

Table 1
Most relevant models that are tested in this work and their performance in terms of Root Mean Square Error (RMSE, Section 2.3.2), and Mean Standard Deviation Percent Error (MSPE, Section 2.3.2).

Model	RMSE	MSPE
XGBoost Regressor	1.05	32.23 %
Random Forest Regressor	1.22	35.57 %
Temporal Fusion Transformer*	2.01	75.69 %
Stochastic Gradient Descent Regressor	1.85	90.99 %
Linear Regressor	1.92	101.01 %
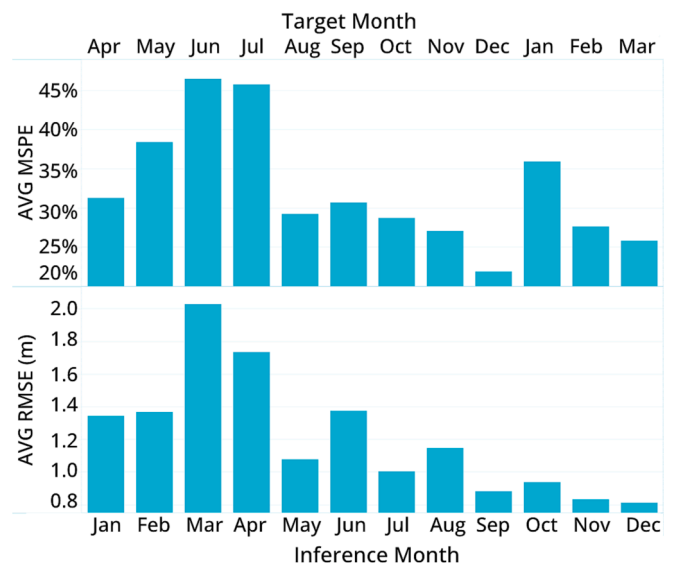
Fig. 5. The average Mean Square Percentage Error (AVG MSPE top) and Root Mean Square Error (AVG RMSE bottom) were calculated by aggregating the results from all wells for each tested month. It is important to note the presence of two x-axes in the figure. The top x-axis represents the 'Target Month' which corresponds to the month for which the prediction of Water Surface Elevation (WSE) is being made. On the other hand, the bottom x-axis represents the 'Inference Month' indicating the month from which the prediction is being made. For instance, the first bar in the figure represents April as the target (predicted) month, with January as the inference month. This means that the prediction for April is made three months in advance, starting from January.

(a) Results for well ID: 3
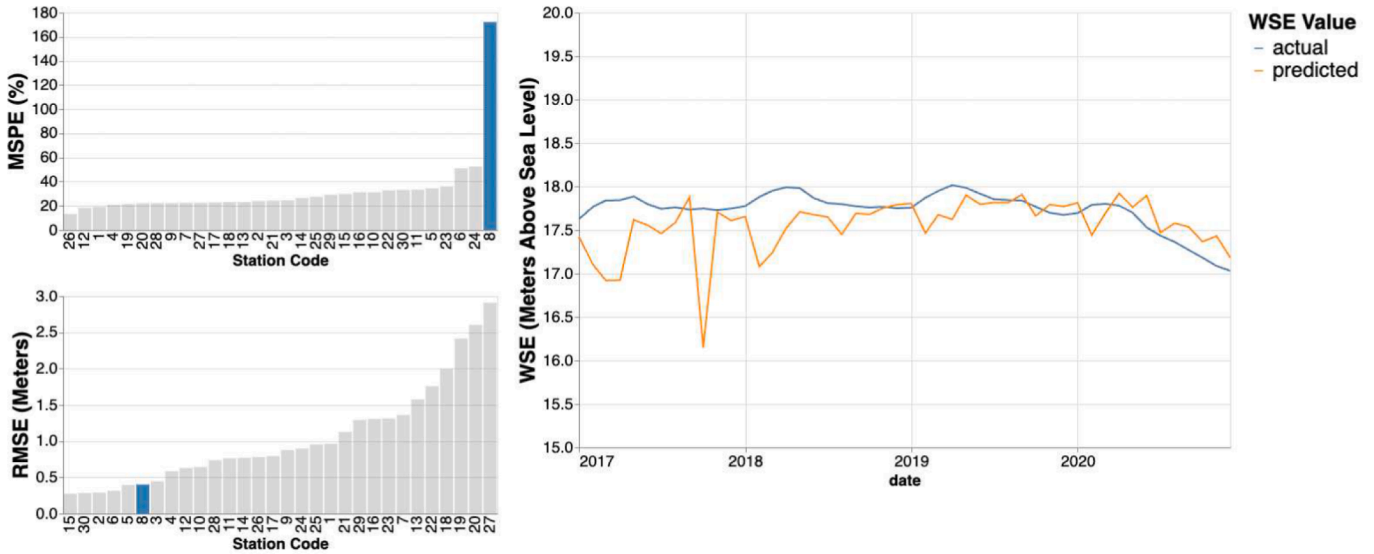
(b) Results for well ID: 8

Fig. 6. Mean Standard Percentage Error (MSPE) and Root Mean Square Error (RMSE) for all wells shown in Fig. 1 with highlighted results to the right, and actual vs predicted values of Water Surface Elevation (WSE) between 2017 and 2020 for a) well ID: 3 and b) well ID: 8. Note that the objective was to minimize RMSE and to keep MSPE below 1. For further information on the meaning of the metrics refer to section 2.3.2.

groundwater withdrawals to keep up with demands from farming and other sectors. In 2014, California adopted the Sustainable Groundwater Management Act (SGMA) to halt the depletion of groundwater resources in the state. Thus, local agencies are in the process of developing plans to limit groundwater withdrawals. Possible options include retiring some cultivated land, converting it into a pasture, agrivoltaic uses, or rainfed production through systems of rotations, incentives, and compensations. In 2021, because drought conditions were so severe, water deliveries to farms were drastically cut, shrinking the irrigated farmland by 304,300 ha across the Central Valley. The loss caused by these cuts is estimated to be $1.7 billion and 14,000 jobs (Medellin-Azuara et al., 2022). Focusing on the area indicated in Fig. 1; and using the datasets described in subsection 2.2.4, it was estimated that the mean annual precipitation to be 22 mm, and the mean potential evapotranspiration to be 19 mm in the area of interest.

2.2. Datasets

The applicability of in-situ measurements for groundwater and its related features has historically been limited in its applicability to real-world modeling as in-situ measurements often introduce bias by relying on easy-to-access locations and are limited in their scope. Thus, a transition to remote sensing data for exogenous meteorological and hydrologic features can help remove some of the biases existing in previous models. For this project, in-situ well measurements throughout the Sacramento River basin were used to represent groundwater levels (Cunningham and Schalk, 2011; CNRA, 2023); as described in the section 'Groundwater Wells'.

Here the model inputs meteorological variables including snow water equivalent (SWE) and evapotranspiration (ET), the wells' data (longitude, latitude, elevation, well depth, well usage, well type), and their water surface elevations. In-puts also included one-hot encoding for all stations, namely, the basins they were located in, as explained
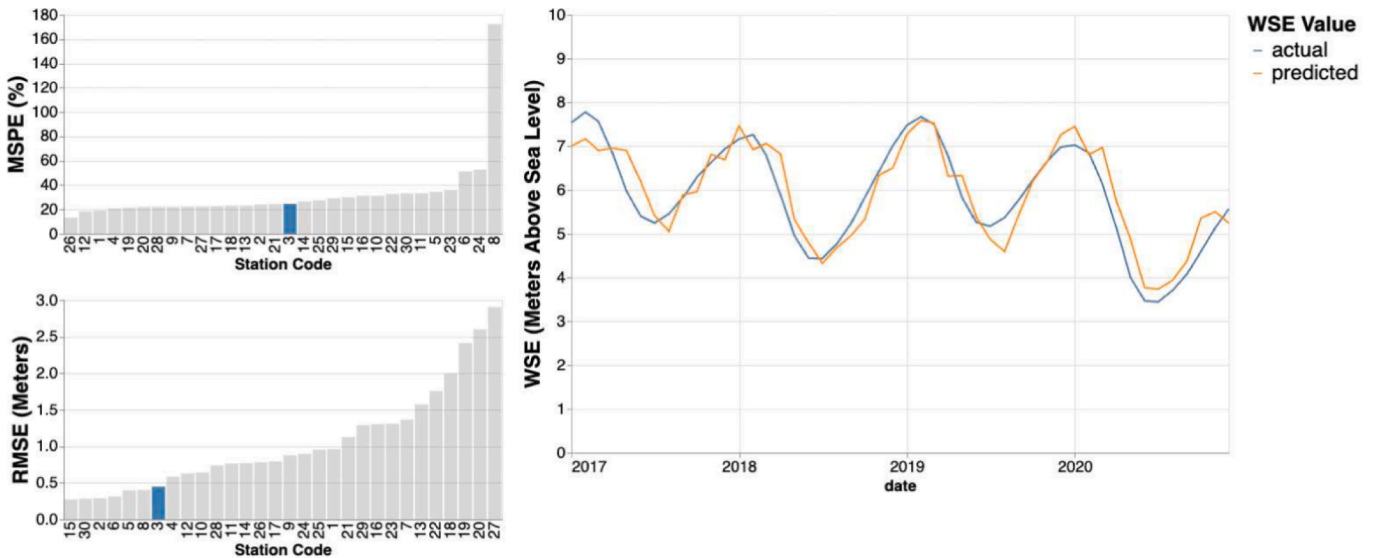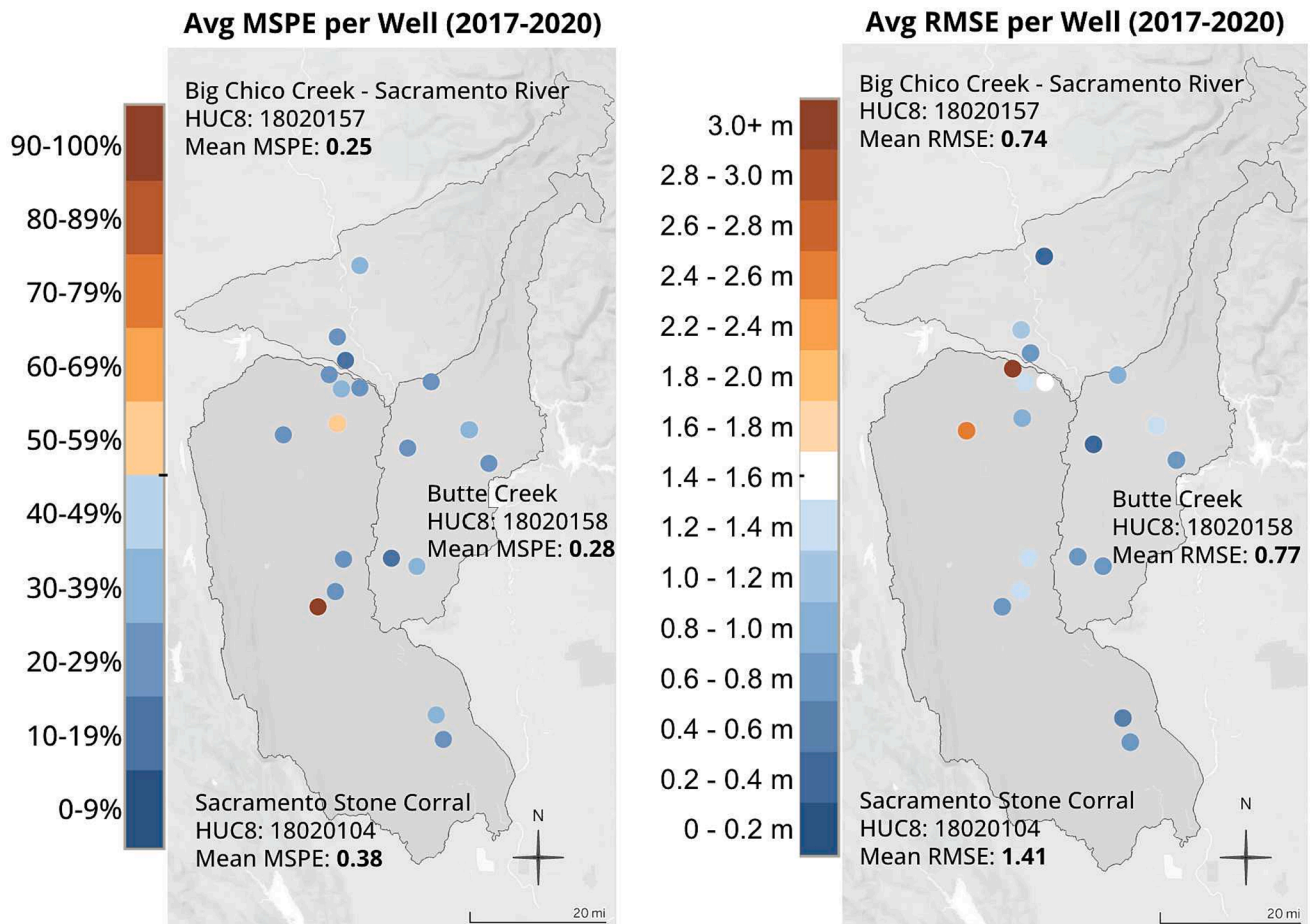
Fig. 7. Average Mean Standard Percentage Error (MSPE) and Root Mean Square Error (RMSE) per well and hydrological region (HUC8) for every tested month (2017–2020).

below. A full list of the variables, or features, used on this project and their sources can be found in appendix A.1.

2.2.1. Groundwater wells

Water Surface Elevation (WSE) measurements for wells located in the Central Valley are taken from the California Natural Resources Agency (CNRA)'s continuous well-level measurement dataset, which contains daily measurements. WSE measurements are relative to groundwater level above the 1988 North American vertical datum (NAVD88) and reported in feet (CNRA, 2023). An initial set of 50 wells with at least 60 months of continuous data was first identified and then filtered for wells with entries at least up to 2020. The final dataset consists of 30 well sites, with data ranging from 2010 to 2020. The final sample of wells used in this study is shown in Fig. 1. Of the 30 sites, only 3 are classified in the CNRA dataset as "irrigation" wells under the field called "well use". Nevertheless, no significant difference in the seasonality of the wells classified as "irrigation" and "observation" wells was observed, so it is assumed that both kinds of wells are part of the same sample. A full list of the CNRA wells used in this study can be found in Appendix A.2.

Here the seasonality was extracted using a Fourier series decomposition. For a further explanation on the seasonality calculation, see appendix A.3. The sample wells are more densely distributed toward the southern part of the Sacramento Valley within three Hydrological Unit Code 8 (HUC8) regions: Big Chico Creek-Sacramento River, Butte Creek, and Sacramento Stone Corral.

The dataset used for this study expresses longitudes and latitudes with 5 decimal points which corresponds to a distance of 1.11 m. There

are several sets of clustered wells that have the same longitudes, latitudes, and elevations in the dataset. Their features, therefore, are also the same. Hence in the calculations, they are only differentiated by their WSE time series.

From the CNRA groundwater wells dataset, the WSE feature was temporally aggregated to create average monthly values. The WSE value, when looking ahead 3-month, was used as this project's target variable. In Fig. 2 we show the monthly time series for two wells together with their seasonality components (see A.3), one (well 28) with a positive seasonality trend, the second (well 19) with a negative seasonality trend. The trend represents the average increase (respectively decrease) from one year to the next of the seasonal component of the WSE.

2.2.2. Evapotranspiration

California's agricultural sector requires an average of 4.2×10^{13} L of water per year, and roughly 80 % of all water used in the Central Valley goes to agriculture (Wong et al., 2021). Hence, having a way to represent the impact of agriculture in the model was imperative to represent the hydrological processes and human activities affecting water table dynamics in the region. For this reason, this project uses evapotranspiration as a proxy for agricultural impact on the groundwater balance (Dari et al., 2022). The evapotranspiration dataset used in this study was taken from the NASA project MODIS16 (Running et al., 2022). The evapotranspiration data has a temporal resolution of 8 days and a spatial resolution of 500 m × 500 m(m) pixels. The mean evapotranspiration over each HUC8 hydrological region was calculated and then averaged monthly to create a time series that was used as the evapotranspiration
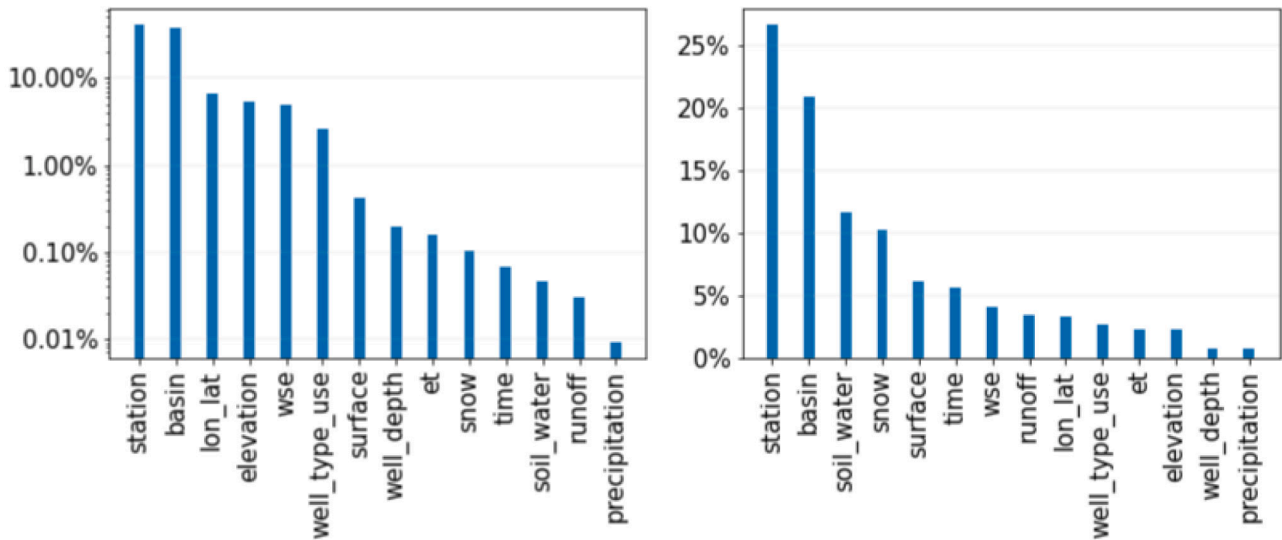
(a) Mean feature importance (across 2017-2020 test years). The importance of a feature is the percentage of total information that it provides. Notice the base 10 log scale of the y axis. Geographical features have higher importance by orders of magnitude.

(b) Mean feature importance after removing seasonality during the test years from 2017 to 2020. Once the effects of seasonality were eliminated, the importance of geographical features, such as longitude/latitude and elevation, significantly decreased. Conversely, meteorological features became more prominent. Note that the y-axis scale in the table is linear.
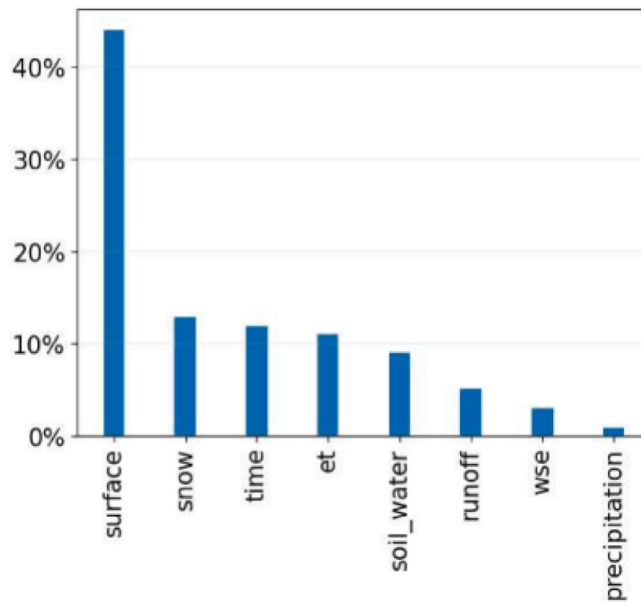
(c) Mean Feature Importance of models trained with individual wells data across 2017-2020 test years and across all wells.

Fig. 8. Feature importance. For simplicity, variables related to the same phenomenon are aggregated. Features aggregations are detailed in Tables A1.

feature.

2.2.3. Snow water equivalent

Snow from the Sierra Nevada serves as one of the main sources of groundwater recharge in the Central Valley. Therefore a snow water equivalent estimate for the Sierra Nevada snowpack from the Western United States UCLA Daily Snow Reanalysis (Fang et al., 2022) was used. Note, this project also incorporates the traditional snow pack-related features further elaborated in the climate variable section below. Snow water equivalent (i.e., the amount of water stored as snow and expressed as the volume of the liquid water equivalent) values are

provided as 1-day averages with a spacial resolution of approximately 500 m. These values were aggregated for each of the HUC8 hydrological regions and then temporally averaged to create monthly means (Fang et al., 2022).

2.2.4. Climate variables

The primary meteorological dataset used as exogenous features were taken from ERA5-Land (Muñoz Sabater et al., 2021), which is a reanalysis of the ERA5 satellite-sourced observation data combined to create model-based estimates. This reanalysis combines physical models with observations and offers a globally complete and reliable dataset. The
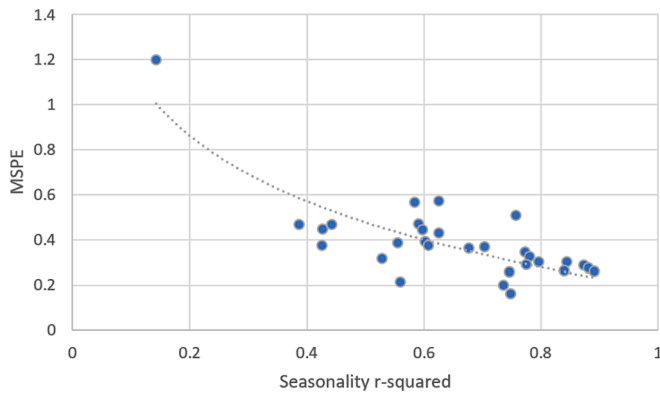
Fig. 9. The plot illustrates the relationship between Mean Standard Percentage Error (MSPE) and seasonality. On the x-axis, the graph shows the increase in the R-squared value of the seasonality regression. As the R-squared value increases, indicating a better fit to regular patterns of water surface elevation, the MSPE decreases. This suggests that the model performs well in capturing and predicting seasonal patterns. However, it may not perform as well in modeling irregular events or variations in water surface elevation.

available information goes back to January 1950, giving a consistent description of the temporal evolution of the climate variables. The ERA5-Land dataset has over 60 different variables, all of which were used at various stages of the modeling process. The dataset's geographical resolution is 9 km × 9 km (or 0.1 × 0.1 degrees) pixels and it is available for up to 1h of temporal resolution. The dataset used in the project can be downloaded directly from the the ERA5-Land site (Store). Similarly to the other supplementary datasets, a monthly average aggregation of the used readings was calculated in order to be able to join the features to the target variable described above. All ERA5-Land variables that were used in the best performing model is presented in Table A1. More detailed description of these specific features can be found in the ERA5 database documentation (ECMWF). These features were selected based on model performance and knowledge of the hydrological processes underlying the nexus between climate variables and water table dynamics. For a more detailed description of the variables see the ERA5-Land documentation (Wiki).

To extract ERA5-Land data, the available interface takes 4 location points and returns the data for a square enclosed by those points. An area that includes the Sacramento basin was extracted but the raw data extends beyond the basin's borders. Thus, for the ERA5-Land meteorological variables, an average value over the watershed was used. The watershed area was used as a proxy for the extent of the groundwater basin area, which was not readily available. So for all wells within the same hydrological unit (HUC8), the monthly values of the meteorological variables, averaged over that unit were used. The average was calculated over all points of the ERA5 data that were in the hydrological unit, within a tolerance of approximately 1 m. This decision is justified by the observation that the groundwater at a given point is influenced by hydrological and meteorological variables such as snow, runoff, solar radiation, and soil water content at locations upstream in their watershed.

2.2.5. Data pipeline: from sources to predictions

So far the datasets and groups of features that seem to have potential to support groundwater levels forecasting have been identified. Fig. 3 illustrates how these diverse group of data sources were processed and brought together in order to create a useful input for a machine learning model capable of predicting future levels of groundwater in the study region.

(a) R-squared = 0.53

(b) R-squared = 0.14

(c) R-squared = 0.89
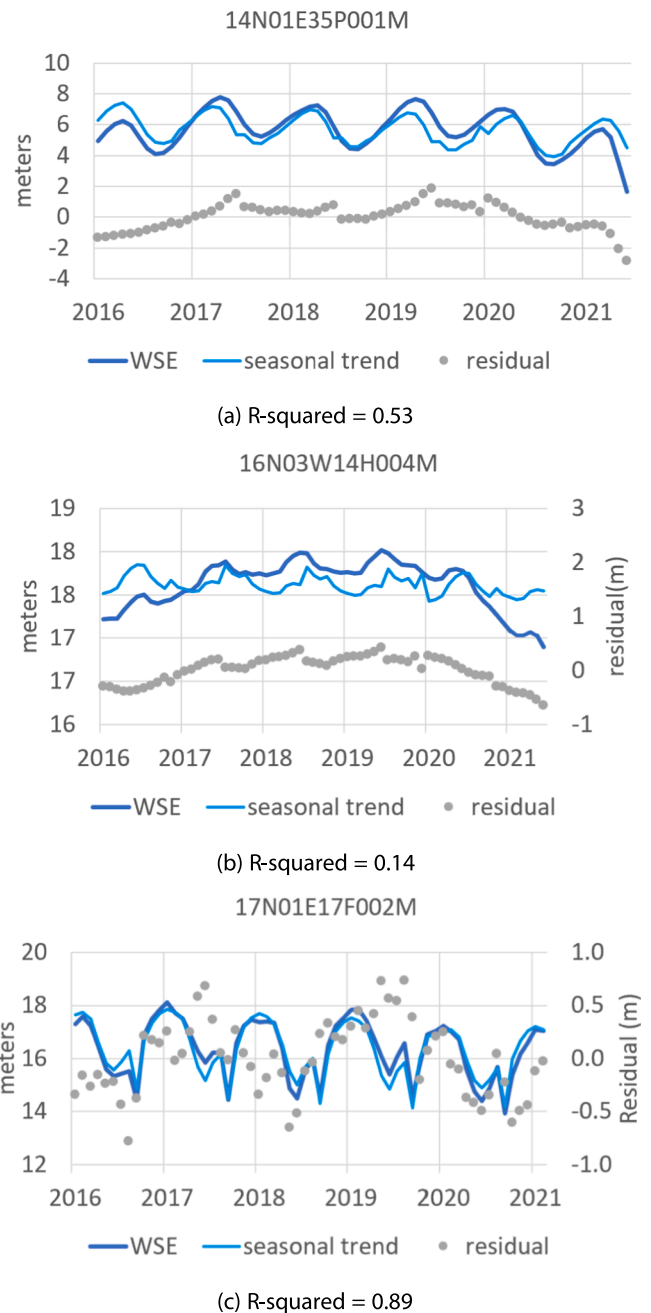
Fig. 10. Seasonality.

3. Problem definition

Here the problem of groundwater level prediction with a machine-learning model using open-source data as input is formulated. Given the historical groundwater level data for each location, learning a regression function that would be used for groundwater prediction is desirable. In particular, let $D=(X,y)$ represent the historical data set, where X is a set of features (representing the characteristics of a well) the objective is to learn a function $f(x)$ such that the error defined in equation 1 is minimized on historical data.

$$\min \sum_{i=1}^{|D|} (f((X_i) - y_i)^2$$

4. Evaluation

In this section, the aim is to evaluate the effectiveness of the proposed model with respect to others. The used dataset have been previously described. Now follows a description of the experimental setup, success metrics, model comparison and the tuning process for the best performing model.

4.1. Experimental setup

To ensure consistency, only wells with at least 60 con secutive monthly observations were chosen to be part of the sample. A specific test set was created using a rolling window approach, covering the months between January 2017 and December 2020. The model was trained on all data preceding the current month in consideration. For example, if the test month is January 2017, the model is trained on data up to December 2016. Since a 3-month forecasting horizon is used, the model predicts water surface elevation (WSE) levels for the target variable month of April 2017. Similarly, for the next test month of February 2017, the model is trained on data up to January 2017 and predicts WSE levels for the target variable month of May 2017. Fig. 4 depicts how the training and test set split was done, and how the rolling windows works.

Out of the initial set of 50 wells, only the 30 wells that recorded water levels during both the training and test pe riods were utilized. This was done to avoid penalizing the model for unfamiliar wells that it hadn't been trained on. When training for a 3-months forecast, each observation of the target variable was paired with features from 3 months earlier, considering that the target variable had already been shifted 3 months into the future.

4.2. Metrics

For evaluation purposes, the following common metrics were adopted: root mean square error (RMSE) and mean absolute error (MAE). These metrics provide a straightforward measure of the vertical distance between the predicted and actual water surface elevation (WSE) values.

Additionally, considering the regular seasonal changes in groundwater level across different wells, and the fact that none of these metrics fully account for this important aspect, another metric is introduced: mean absolute percentage error (MAPE). The formula for MSPE is as follows:

$$MSPE = \frac{predicted - actual}{\sigma_n(actual)}$$

Here, σ_n represents the historical standard deviation of an n-month change in WSE, where n corresponds to the number of months being forecasted. MSPE measures the error as a fraction of the magnitude of the fluctuations of a given well, and thus allows for a fairer comparison of errors among wells.

The goal is to minimize both RMSE and MSPE, although the emphasis may vary depending on whether the focus is on optimizing the actual error in water level (RMSE) or the error relative to the typical fluctuations in water level (MSPE).

4.3. Models comparison

Several models were tested for the forecasting of WSE levels. The initial testing stages involved linear regression models, such as Bayesian Ridge regressions, and support vector machines (SVM) (Zhou et al., 2017). In addition, runs of Auto-Regressive Integrated Moving Average (ARIMA) (Bagher Shirmohammadi and Vafakhah, 2013) models were done, both before and after extracting seasonality, considering various scenarios such as weighting the exogenous features and accounting for correlations. Although these models effectively captured the time series structure in an intuitive manner, they did not yield the best MSPE (Mean

Squared Prediction Error) scores.

Random Forest and Gradient Boosting. A variety of en semble based decision tree models were also compared with the Random Forest Regressor used as the baseline model in this category (Moghaddam and Rahmati, 2020). Gradient boosted decision tree architectures were evaluated against the Random Forest Regressor including XGBoost, Catboost, Gradient Boosting Machine (GBM), and Light Gradient Boosting Machine (LGBM). The highest performing model architecture in this category was XGboost which follows a gradient boosting framework. See Fig. 3 for specific hyperparameters used in final model.

Deep Learning Models. Deep learning models were the final family of models tested, including the Long Short-Term Memory model (LSTM), and a Temporal Fusion Transformer (TFT). LSTM has been used in forecasting groundwater in prior work, see for example (Zhang et al., 2018). TFT is a promising recent architecture that marries LSTM with transformers (Lim et al., 2019). Both are recursive neural networks that assess the importance of past observations in order to determine future observations without requiring a fixed look-back window.

Most of the forecasting models were constructed at the basin level, resulting in a single model for all wells in the dataset, but efforts were also made to model at the well level using a variety of time series models, where a different model was run for each well. For those models, errors were calculated as an average of all individual wells' errors, and were found to not outperform other approaches at the average level. While the former approach allows us to forecast WSE for any new wells in the area, the latter approach can be more closely tuned to each individual well. All models were trained in Python, on Google Colab using open source libraries including Scikit-Learn and PyTorch. The notebooks are available in the project repository (Ellestad et al., 2022). It is important to note that many more models, algorithms and architectures have been studied to tackle inference problems related to the forecast of groundwater levels. These went beyond the scope of this project for several reasons. For a detailed literature review of these efforts, please refer to (Tao et al., 2022).

4.4. Hyperparameter tuning

Several feature engineering and data pre-processing steps in conjunction with the aforementioned model architectures were evaluated. These steps included: (1) incorporating lagged versions of exogenous variables (Yanti and Rahardiantoro, 2019), (2) performing feature normalization (Han et al., 2012); and (3) applying dimensionality reduction through Principal Component Analysis (PCA) (Sun et al., 2021). Among the listed methods, only feature normalization using a Min Max Scalar approach, which bounds each feature within the range of [0, 1], demonstrated improved performance. The inclusion of lagged variables led to a reduction in the overall size of the training dataset since earlier timestamps lacked sufficient prior data for inclusion. Not to employing PCA was an intentional choice made to maintain the explainability of the results, as transforming the feature set into a smaller set of projected dimensions would compromise this aspect.

5. Results and discussion

The ensemble based models produced the best MSPE scores compared to the other families of models. The XGBoost regressor model was the best with an MSPE score of 32.23\%, when using a 3-month forecasting horizon. Noticeably, the deep learning models and the TFT had the worst performance, most likely due to the fact that it requires considerable amounts of training data to be effective, an amount that was not available in this case. Table 1 shows the total RMSE and MSPE for the test period of 2017 to 2020 obtained for the most relevant models.

This study introduces a novel way to predict future WSE levels and to measure forecast error (MSPE) for a set of wells with different amplitudes of seasonal fluctuations for the Sacramento River Basin. MSPE is

useful when comparing results across wells at a given time. In these experiments best inference of future WSE levels in the Sacramento Valley was achieved by the XGBoost model for a 3-month look ahead period. Overall, it is more difficult to predict water levels for the summer months (see average MSPE and RMSE per prediction month in Fig. 5). It is speculated that this might be due to the irregularity of withdrawals, and overall stronger human intervention associated with crop-specific irrigation water use, the proximity of the well to water-depleted areas, or the condition of the water pump, in addition to the seasonal fluctuation of the WSE. Therefore, a better proxy feature accounting for the effect of human activity and water usage is needed to further improve the model. Fig. 5 shows the average MSPE and RMSE for each month of all wells in the test set over all test years (2017–2020). Since February, March and April were the worst performing months, March and April were the worst performing months for the model to predict WSE from, May, June and July are the hardest months to forecast, given that a 3-month forecasting horizon is used.

Fig. 6 shows RMSE and MSPE values for all 30 stations as well as an example time-series of a well located in the Sacramento Stone Corral sub-basin (HUC8 18020104), Well 3. Station 3 has both good RMSE and MSPE relative to other wells.

The worst MSPE performance was found for well station 8, which also had the sixth best performance in terms of RMSE (Fig. 6). The model's predicted fluctuations of WSE for this well were quite close to the actual fluctuations in absolute terms, hence the low RMSE. On the other hand, since in this well the WSE varies very little over time, the small RMSE was still quite large compared to the fluctuation in WSE levels, resulting in a high MSPE.

A look at the geographical distribution of the wells and their overall performance shows that wells in the Big Chico Creek - Sacramento River sub-basin (HUC8 18020157) and the Butte Creek sub-basin (HUC8 18020158) generally had better performance than those located in the Sacramento Stone Corral sub-basin (HUC8 18020104), which are towards the bottom of the valley (Fig. 7). This may be explained by their proximity to the Sierra Nevada. Moreover, WSE and SWE levels were noticeably lower in the Sacramento Stone Coral sub-basin HUC8 18,020,104 than in the other two watersheds, suggesting the occurrence of a more intense groundwater withdrawal in this area, a process that is only indirectly accounted for (through evapotranspiration) in the presented model. For more detail, feature importance is explored.

5.1. Feature importance

Feature importance in the XGBoost model is measured by the percentage of the total information that is provided by each feature. Feature importance was generally stable across all test months and years, so the rankings in Fig. 8 a show the mean feature importance values for all models trained in the XGBoost experiments.

In order to get a better idea of the relative importance of various feature types, the importance of features that relate to the same phenomenon were aggregated. In Fig. 8a and Fig. 8b, all features related to snow (snow cover, snow depth, snow water equivalent, snow density, snow albedo, snow melt) are aggregated under the feature name 'snow'. Similarly all 4 layers of volumetric soil water are aggregated under the name 'soil water', etc. See appendix for definitions of other aggregates.

Fig. 8a relates to the original model. Note that the y-axis is based in log base 10. In this model, features with the highest importance, such as location, elevation, and history of values are all well-related. However, it is still unclear what specifically about those features is the cause as wells in the same basin will have the same meteorological features. Exogenous meteorological and hydrological features were expected to greatly impact the results (groundwater levels are expected to depend on precipitation in the previous months,) but were shown to have very little importance in general.

One may surmise that some geographical features, such as for example elevation are correlated with hydrometeorological features (e.

g., the snow features), however, similar results were observed after features were lagged, scaled, and had PCA performed to reduce the number of dimensions.

The same process was repeated after removing the seasonality and the linear trend from each well's time series of WSE. While station and basin remained the most important features across all months, other features' importance was not as stable over time. The aggregated features had a more stable relative importance and exhibited higher importance of hydrometeorological features (soil water, snow, surface, etc.), Fig. 8b. This is consistent with the fact that well-related features are the most important factors governing the seasonal fluctuations of WSE, while meteorological features impact deviations from regular seasonality patterns. The low importance of precipitation in both analyses (i.e., with and without detrending) suggests that fluctuations in WSE may be more strongly controlled by recharge from snowmelt than precipitation.

It is worth noting that the most important features for the model were related to the location of each individual well. This could be because the model is able to generalise over the entire Sacramento Basin, so a potential use for this kind of forecast could be the prediction of WSE levels in locations within the basin where there is no monitoring at the moment.

Nevertheless, the current ranking of model's features does not reflect the expected importance of the hydrological processes. For this reason, several XGBoost models were trained using only a single well time-series at a time. It was observed that the average MSPE decreased by 0–2 % and the average RMSE decreased by 0–0.15 m. The feature importance distribution, however, changed significantly, as observed in Fig. 8c.

5.2. MSPE versus time and seasonality

While mean MSPE values vary in space (i.e., across wells and are lower in the hydrological units that are closer to the Sierra Nevada), the MSPE value ranged between 15 % and 70 % over the 4 year period used for testing (2017–2020). Even though numerically the range appears to be large (55 %), it implies that the model is consistently able to predict well within a standard deviation of the expected value of the target variable. In other words, even during the hardest periods for a forecast, the model was able to outperform naive estimators.

Another aspect of MSPE is that wells with less seasonal irregularity, as measured by the r-squared of the regression against their periodicity (see Appendix A.3), display a lower MSPE, which indicates that the model captures seasonality, but other random fluctuations are more difficult to model. In Fig. 9 each dot represents one well. The outlier is well 8 which has the lowest seasonality and therefore also a very high MSPE due to its low variability.

It is important to note that the methodology followed in this work is transferable to any other region where the same data is available. Since all the data for the input variables were taken from global data products such as MODIS and ERA-5 Land, all relevant features are readily available for any region in the world. Nevertheless, since the methodology is based on supervised learning, it is imperative to have good quality data for the target feature. In other words, in order to transfer this work to other places in the world it is necessary to have reliable and robust data sets representing historic groundwater levels at the same temporal resolution. Therefore, the main limitation for the scaling up of this work is groundwater levels data availability.

6. Conclusion

The goal of this project was to develop and fine-tune a machine learning model that could forecast well water levels in order to predict groundwater levels for the Sacramento Valley. In addition, this model may be used to forecast the changes in a new well in one of the three watershed areas, given that well's geographic position, elevation, depth, and type, as long as a proxy for historical WSE, such as that of a nearby

well, or an average for the sub-basin, is provided.

Ultimately, the XGBoost model predicting 3 months ahead provided the most accurate and precise results, with an average MSPE of 32.23 %, with an average RMSE of 1.05 m. Overall, the XGBoost model was able to pick up seasonal patterns with well-specific related features being more important than exogenous meteorological and hydrological features.

Using more accurate data sources for those exogenous features and including other aspects that affect groundwater levels is something that can be improved upon in future iterations of the study.

Additionally, there are other hydrological factors not yet accounted for in the dataset. For instance, because wells differ in the amount of energy required for water withdrawal, there are situations where wells that are further away but easier to pump (i.e., they require less energy) are preferentially used over wells that are closer but water withdrawals from them require more energy. This means that well levels are not necessarily the most accurate way of depicting local usage and finding a way to account for this effect could improve the representation for the impact of human action. Collectively, the results presented in this study show the potential offered by artificial intelligence methods in the modeling of groundwater dynamics and the water table dependence on hydrometorological drivers.

It is important to note that climate change will have relevant impacts on the forecasting capabilities of the proposed models, but the definition of those effects go beyond the scope of this project. Therefore, the authors propose that future work should look into different climate scenarios by using data sets such as CMIP6 (O'Neill et al., 2016).

Finally, the authors believe that the methodology proposed here is accessible for water management and agriculture organizations aiming to improve their water security resilience and preparedness. From the creation of data-driven public policy at the regional level, to the development of sustainable water management practices for individual agricultural practitioners, the forecasting capability of the proposed model can harness the potential of data to help people and organisations achieve their water security goals.

CRediT authorship contribution statement

Gabriela May-Lagunes: Methodology, Software, Validation, Investigation, Visualization, Project administration, Writing – original draft, Writing – review & editing. **Valerie Chau:** Methodology, Software, Validation, Investigation, Visualization, Writing – original draft, Writing – review & editing. **Eric Ellestad:** Methodology, Software, Validation, Investigation, Visualization, Writing – original draft, Writing – review & editing. **Leyla Greengard:** Methodology, Software, Validation, Investigation, Visualization, Writing – original draft, Writing – review & editing. **Paolo D'Odorico:** Conceptualization, Methodology, Resources, Writing – review & editing, Supervision, Funding acquisition. **Puya Vahabi:** Supervision. **Alberto Todeschini:** Conceptualization, Methodology, Resources, Supervision. **Manuela Girotto:** Conceptualization, Methodology, Resources, Writing – review & editing, Supervision, Funding acquisition.

Declaration of competing interest

The authors declare that they have no known competing financial interests or personal relationships that could have appeared to influence the work reported in this paper.

Data availability

All data and code used is open to the public and referenced in the manuscript.

Acknowledgements

A. Appendix

A.1. Meteorological and descriptive feature names and definitions

Table A1 has the list of all meteorological variables used as exogenous features, descriptive variables giving information about the wells location and use, and the aggregates they to in the feature importance rankings reported previously in Fig. 8. With the exception of Snow Water Equivalent (SWE), which comes from the the Western United States UCLA Daily Snow Reanalysis project Fang et al., 2022, all other features below are from ERA5-land Store.

Table A1
List of all variables used. Left to right columns indicates the variable as defined by the native product, its definition, the data source for these variables, and the assigned aggregate name to explain feature importance, respectively.

Variable name	Definition	Data source	Aggregate name *
ro	runoff	ERA-5 Land (Store)	runoff
ssro	subsurface runoff	ERA-5 Land (Store)	
sro	surface runoff	ERA-5 Land (Store)	
e	evaporation	ERA-5 Land (Store)	et
et	evapotranspiration	MODIS16A (Running et al., 2022)	
slhf	surface latent heat flux	ERA-5 Land (Store)	surface
ssr	surface net solar radiation	ERA-5 Land (Store)	
str	surface net thermal radiation	ERA-5 Land (Store)	
sshf	surface sensible heat flux	ERA-5 Land (Store)	
ssrd	surface solar radiation downwards	ERA-5 Land (Store)	
strd	surface thermal radiation	ERA-5 Land (Store)	
asn	snow albedo	ERA-5 Land (Store)	snow
snowc	snowcover	ERA-5 Land (Store)	
rsn	snow density	ERA-5 Land (Store)	
sde	snow depth	ERA-5 Land (Store)	
sd	snow depth water equivalent	ERA-5 Land (Store)	

(continued on next page)

Table A1 (*continued*)

Variable name	Definition	Data source	Aggregate name *
sf	snowfall	ERA-5 Land (Store)	
smlt	snowmelt	ERA-5 Land (Store)	
swe	snow water equivalent	UCLA Daily Snow Reanalysis project (Fang et al., 2022)	
swvl1	volumetric soil water layer 1	ERA-5 Land (Store)	soil_water
swvl2	volumetric soil water layer 2	ERA-5 Land (Store)	
swvl3	volumetric soil water layer 3	ERA-5 Land (Store)	
swvl4	volumetric soil water layer 4	ERA-5 Land (Store)	
tp	total precipitation	ERA-5 Land (Store)	precipitation
elevation	elevation from sea level	CNRA (CNRA, 2023)	elevation
longitude	longitude	CNRA (CNRA, 2023)	lon_lat
latitude	latitude	CNRA (CNRA, 2023)	
standalone	well is not part of a well cluster	CNRA (CNRA, 2023)	well_type_use
cluster	well is part of a well cluster	CNRA (CNRA, 2023)	
irrigation	well used for irrigation	CNRA (CNRA, 2023)	
observation	well is used for observation	CNRA (CNRA, 2023)	
station code CNRA well unique code	CNRA (CNRA, 2023)	station	
huc8	CNRA hydrologic unit unique code	CNRA (CNRA, 2023)	huc8
basin	CNRA unique basin code	CNRA (CNRA, 2023)	basin
well depth	CNRA well max depth with respect to sea level in meters CNRA (CNRA, 2023)	well_depth	
time	CNRA timestamp (UTC) of wse measurements	CNRA (CNRA, 2023)	time
wse	CNRA water elevation level (project target variable)	CNRA (CNRA, 2023)	wse
residual	seasonality residual	calculated as described in A.3	residual

A.2. Well descriptions

Table A2 reports the information about the 30 wells in the dataset.

Table A2
The information about the 30 wells in the dataset is reported. The columns include Well Id, Station Code, HUC8, Basin, Well Use (irrigation or observation), Well Type (nested or single), Latitude, and Longitude. Well Id, as showed in Fig. 1 is the assigned numbering for the 30 wells in the final dataset. Other columns are California Natural Resources Agency (CNRA) station code; HUC to which the well belongs; Basin to which the well belongs; Well Use - irrigation or observation; Well Type - whether the well is part of a part of a nested/multi-completion well or a single well; Latitude; Longitude.

Well Id	Station Code	HUC8	Basin	Well Use	Well Type	Latitude	Longitude
1	13N01E24G003M	18,020,104	5–021.62	Observation	Multi	38.9605	−121.8102
2	13N01E24G004M	18,020,104	5–021.62	Observation	Multi	38.9605	−121.8102
3	14N01E35P001M	18,020,104	5–021.52	Observation	Multi	39.012435	−121.829041
4	14N01E35P002M	18,020,104	5–021.52	Observation	Multi	39.012435	−121.829041
5	14N01E35P003M	18,020,104	5–021.52	Observation	Multi	39.012435	−121.829041
6	14N01E35P004M	18,020,104	5–021.52	Observation	Multi	39.012435	−121.829041
7	16N02W05B001M	18,020,104	5–021.52	Observation	Multi	39.275273	−122.105677
8	16N03W14H004M	18,020,104	5–021.52	Observation	Multi	39.241473	−122.153517
9	16N03W14H005M	18,020,104	5–021.52	Observation	Multi	39.241473	−122.153517
10	17N01E17F002M	18,020,158	5–021.70	Observation	Multi	39.32572	−121.882942
11	17N01E17F003M	18,020,158	5–021.70	Observation	Multi	39.32572	−121.882942
12	17N01W10A001M	18,020,158	5–021.70	Observation	Multi	39.343775	−121.951948
13	17N02W09H003M	18,020,104	5–021.52	Observation	Multi	39.341681	−122.083787
14	17N02W09H004M	18,020,104	5–021.52	Observation	Multi	39.341681	−122.083787
15	20N01E18L003M	18,020,158	5–021.70	Observation	Multi	39.577063	−121.908277
16	20N02E09G001M	18,020,158	5–021.57	Observation	Single Well	39.615453	−121.739123
17	20N03E31M001M	18,020,158	5–021.57	Observation	Single Well	39.54458	−121.687321
18	20N03W07E001M	18,020,104	5–021.52	Observation	Multi	39.604892	−122.249484
19	20N03W07E002M	18,020,104	5–021.52	Observation	Multi	39.604892	−122.249484
20	20N03W07E003M	18,020,104	5–021.52	Observation	Multi	39.604892	−122.249484
21	21N02W01F001M	18,020,104	5–021.52	Observation	Multi	39.704336	−122.038614
22	21N02W01F002M	18,020,104	5–021.52	Observation	Multi	39.704336	−122.038614
23	21N02W04G005M	18,020,104	5–021.52	Observation	Multi	39.703325	−122.091003
24	21N02W33M003M	18,020,104	5–021.52	Observation	Multi	39.629906	−122.100662
25	22N01E35E001M	18,020,158	5–021.57	Irrigation	Single Well	39.718223	−121.843211
26	22N02W15C002M	18,020,157	5–021.51	Observation	Multi	39.763431	−122.077156
27	22N02W30H002M	18,020,104	5–021.52	Observation	Multi	39.73245	−122.123331
28	23N02W28N001M	18,020,157	5–021.51	Observation	Multi	39.811489	−122.102064
29	23N02W28N002M	18,020,157	5–021.51	Observation	Multi	39.811489	−122.102064
30	24N02W01L002M	18,020,157	5–021.56	Observation	Multi	39.961965	−122.03913

A.3. Calculating seasonality

Seasonality was extracted using a Fourier series decomposition of WSE. Compared to the method of calculating the average value of WSE for each month over the entire period, this approach has the advantage of estimating the trend of the periodic changes. For example not only does this approach show that the highest level of WSE for any given year is achieved in April, but also, that over the years the WSE level for April has been decreasing. In addition, this method provides a better approximation of seasonality as it results smaller residuals. The Fourier decomposition follows the equation.

$$y(t) = at + \sum_{i=1}^{10}(\beta_i \sin(t) + \gamma_i \cos(t)) + \in_t \quad (3)$$

where y(t) represents WSE at time t, at is the linear component (trend,) $\left(\sum_{i=1}^{10}(\beta_i \sin(t) + \gamma_i \cos(t))\right)$ is the periodic seasonal component, and $\in_t$ the residual at time t. The coefficients α, β_i and γ_i are estimated by running a linear regression. The below show the decompositions for wells 3 and 8 which were discussed in the text and for well 10 which had the highest r-squared. By observing that there is a pattern in the residuals for the first two wells, one can surmise that other factors are influencing their WSE's. The residuals of the third well appear to be much closer to a random walk.

It is important to note that the second well in Fig. 10 shows that in that particular well the hydrologic signal did not have a strong seasonal behavior, therefore the groundwater level fluctuations have a different origin, such as hydrological, meteorological or human, than just the seasonal water cycle. This case illustrates the strength of our methodology since it takes into account all the exogenous factors described in the text. From a mathematical point of view, the seasonality calculation is solely based on the past history of water level fluctuations whereas our methodology includes other factors. In this particular case, a close look at the graph shows large deviations from seasonality during the drought periods of 2016 and 2021, during which according to the US Drought Monitor large areas had exceptional droughts.

A.4. XGBoost model full list of hyperparameters used

Table A4

Hyperparameter	Value
booster	'gbtree' (default)
verbosity	1 (default)
validate_parameters	'True' (default)
maxthreads	Not specified (default)
disable_default_eval_metric	'False' (default)
num_feature	Not specified (default)
learning_rate	0.01
min_split_loss	0 (default)
max_depth	10
min_child_weight	1 (default)
maxthreads	Not specified (default)
max_delta_step	0 (default)
subsample	1 (default)
sampling_method	'uniform' (default)
colsample_bytree	0.7
colsample_bylevel	1 (default)
colsample_bytree	1 (default)
lambda	1 (default)
alpha	0 (default)
tree_method	'auto' (default)
scale_pos_weight	1 (default)
refresh_leaf	1 (default)
process_type	'default' (default)
grow_policy	'depthwise' (default)
max_leaves	0 (default)
max_bin	256 (default)
predictor	'auto' (default)
num_parallel_tree	1 (default)
objective	'reg:squarederror' (default)

References

Bagher Shirmohammadi, V.M.A.M., Vafakhah, M., 2013. Application of several data-driven techniques for predicting groundwater level, Water Resour. Manage 27, 419–432.

Barzegar, R., Fijani, E., Moghaddam, A., Tziritis, E., 2017. Forecasting of groundwater level fluctuations using ensemble hybrid multi-wavelet neural network-based models. Sci. Total Environ. 599–600, 20–31.

CNRA, Continous groundwater level measurements, https://data. cnra.ca.gov/dataset/continuous-groundwater-level-measurements, 2023.

Condon, L., Atchley, A., Maxwell, R., 2020. Evapotranspiration depletes groundwater under warming over the contiguous united states. Nat. Commun. 11, 873.

Cunningham, W.L., Schalk, C.W., 2011. Groundwater technical procedures of the U.S. geological survey. U.S Geological Survey Techniques and Methods 1–A1, 151.

Dari, J., Quintana-Seguí, P., Morbidelli, R., Saltalippi, C., Flammini, A., Giugliarelli, E., Escorihuela, M., Stefan, V., Brocca, L., 2022. Irrigation estimates from space: Implementation of different approaches to model the evapotranspiration contribution within a soil-moisture- based inversion algorithm. Agric. Water Manage. 265, 107537.

de Moraes Takafuji, E., da Rocha, M., Manzione, R., 2019. Groundwater level prediction/forecasting and assessment of uncertainty using sgs and arima models: A case study in the bauru aquifer system (brazil). Nat. Resour. Res. 9, 487–503.

Ebrahimi, R.S., Eslamian, S., Zareian, M.J., 2022. Groundwater level prediction using gms and svr models under rcp scenarios in the future period (case study: Talesh plain). Theor. Appl. Climatol. 151 (1–2), 433–447.

ECMWF, Parameter database, https://codes.ecmwf.int/grib/ param-db/, N/A.

E. Ellestad, L. Greengard, G. May-Lagunes, V. Chau, Forecasting ground water levels in the central valley of california repository, 2022. URL: https://github.com/eric1650/ca-watertable-forecast.

Fang, Y., Liu, Y., Margulis, S., 2022. A western united states snow reanalysis dataset over the landsat era from water years 1985 to 2021. Sci. Data 9, 677.

C. Faunt, R. Hanson, K. Belitz, Groundwater availability of the central valley aquifer, california: U.s. geological survey professional paper 1766 (2009) 225.

Goodarzi, M., 2020. Application and performance evaluation of time series, neural networks and hartt models in predicting groundwater level changes, Najafabad Plain, Iran, Sustain. Water Resour. Manage. 6, 1–10.

J. Han, M. Kamber, J. Pei, 3 - data preprocessing (2012) 83–124.

K. T. Hancock, J.T., Survey on categorical data for neural networks, Big Data 7 (2020).

B. Li, M. Rodell, Chapter 11 - groundwater drought: environmental controls and monitoring (2021) 145–162.

B. Lim, S. Arik, N. Loeff, T. Pfister, Temporal fusion transformers for interpretable multi-horizon time series forecasting, arXiv (2019).

Liu, P., Famiglietti, J., Purdy, A., et al., 2022. Groundwater depletion in california's central valley accelerates during megadrought. Nat. Commun. 13, 7825.

J. Medellin-Azuara, A. Escriva-Bou, J. M. Rodriguez-Flores, S. A. Cole, J. Abatzoglou, J. H. Viers, N. Santos, D. A. Sumner, Economic impacts of the 2020–22 drought on california agriculture; report prepared for the california department of food and agriculture, UC Merced Water System Management Lab (2022).

A. H. Z. K. D.D. Moghaddam, O. Rahmati, A modeling comparison of groundwater potential mapping in a mountain bedrock aquifer: Quest, garp, and rf models, Water 12 (2020) 679.

Muñoz Sabater, J., Dutra, E., Agustí-Panareda, A., Albergel, C., Arduini, G., Balsamo, G., Boussetta, S., Choulga, M., Harrigan, S., Hersbach, H., Martens, B., Miralles, D.G., Piles, M., Rodríguez-Fernández, N.J., Zsoter, E., Buontempo, C., Thépaut, J.-N., 2021. Era5-land: a state-of-the-art global reanalysis dataset for land applications. Earth Syst. Sci. Data 13, 4349–4383.

O'Neill, B.C., Tebaldi, C., van Vuuren, D.P., Eyring, V., Friedlingstein, P., Hurtt, G., Knutti, R., Kriegler, E., Lamarque, J.-F., Lowe, J., Meehl, G.A., Moss, R., Riahi, K., Sanderson, B.M., 2016. The scenario model intercomparison project (scenariomip) for cmip6. Geosci. Model Dev. 9, 3461–3482.

Rosa, L., Rulli, M.C., Davis, K.F., Chiarelli, D.D., Passera, C., D'Odorico, P., 2018. Closing the yield gap while ensuring water sustain- ability. Environ. Res. Lett. 13, 104002.

S. Running, Q. Mu, M. Zhao, Mod16a2 modis/terra net evapotranspiration 8-day l4 global 500m sin grid v006, NASA EOSDIS Land Processes DAAC. (2022).

C. C. D. Store, Copernicus climate data store overview, https://cds.climate.copernicus. eu/cdsapp#!/dataset/ reanalysis-era5-land-monthly-means?tab=overview, N/A.

Sun, X., Zhou, Y., Yuan, L., Li, X., Shao, H., Lu, X., 2021. Integrated decision- making model for groundwater potential evaluation in mining areas using the cusp catastrophe model and principal component analysis. J. Hydrol.: Reg. Stud. 37, 100891.

Tao, H., Hameed, M.M., Marhoon, H.A., Zounemat-Kermani, M., Heddam, S., Kim, S., Sulaiman, S.O., Tan, M.L., Sa'adi, Z., Mehr, A.D., Allawi, M.F., Abba, S., Zain, J.M., Falah, M.W., Jamei, M., Bokde, N.D., Bayatvarkeshi, M., Al-Mukhtar, M., Bhagat, S. K., Tiyasha, T., Khedher, K.M., Al-Ansari, N., Shahid, S., Yaseen, Z.M., 2022. Groundwater level prediction using machine learning models: A comprehensive review. Neurocomputing 489, 271–308.

Taylor, L.L., Quirk, J., Thorley, R.M.S., Kharecha, P.A., Hansen, J., Ridgwell, A., Lomas, M.R., Banwart, S.A., Beerling, D.J., 2016. Enhanced weathering strategies for stabilizing climate and averting ocean acidification. Nat. Clim. Chang. 6, 402–406.

USGC, Hydrologic unit maps, https://water.usgs.gov/GIS/huc.html, 2023.

Wada, Y., Flörke, M., Hanasaki, N., Eisner, S., Fischer, G., Tram-berend, S., Satoh, Y., van Vliet, M.T.H., Yillia, P., Ringler, C., Wiberg, D., 2016. Modeling global water use for the 21st century: Water futures and solutions (WFAS) initiative and its approaches. Geosci. Model Dev. 9, 175–222.

E. C. Wiki, Era5-land: data documentation, https://confluence. ecmwf.int/display/CKB/ ERA5-Land%3A+data+documentation, N/A.

A. J. Wong, Y. Jin, J. Medellin-Azuara, K. T. Paw, E. R. Kent, J. M. Clay, F. Gao, J. B. Fisher, G. Rivera, C. M. Lee, K. S. Hemes, E. Eichelmann, D. D. Baldocchi, S. J. Hook, Multiscale assessment of agricultural consumptive water use in California's central valley (2021).

Yanti, Y., Rahardiantoro, S., 2019. Stepwise approach in lagged variables time series modeling: A simple illustration. IOP Conf. Ser.: Mater. Sci. Eng. 621, 012009.

Zhang, X., Dong, F., Chen, G., Dai, Z., 2023. Advance prediction of coastal groundwater levels with temporal convolutional and long short-term memory networks. Hydrol. Earth Syst. Sci. 27, 83–96.

Zhang, J., Zhu, Y., Zhang, X., Ye, M., Yang, J., 2018. Developing a long short- term memory (lstm) based model for predicting water table depth in agricultural areas. J. Hydrol. 561, 918–929.

Zhou, T., Wang, F., Yang, Z.Y., 2017. Comparative analysis of ann and svm models combined with wavelet preprocess for groundwater depth prediction. Water 9, 781.